Cross-sections for heavy atmospheres: H_2O self-broadening

Lara O. Anisman[a], Katy L. Chubb[b], Quentin Changeat[a], Billy Edwards[c,a],
Sergei N. Yurchenko[a], Jonathan Tennyson[a], Giovanna Tinetti[a]

[a] *Department of Physics and Astronomy, University College London, Gower Street, London, WC1E 6BT, United Kingdom*
[b] *Centre for Exoplanet Science, University of St Andrews, North Haugh, St Andrews, KY16 9SS, United Kingdom*
[c] *AIM, CEA, CNRS, Université Paris-Saclay, Université de Paris, Gif-sur-Yvette, F-91191, France*

Abstract

The discovery of super-Earth and mini-Neptune exoplanets means that atmospheric signals from low-mass, temperate exoplanets are being increasingly studied. The signal acquired as the planet transits its host star, known as the *transit depth*, is smaller for these planets and, as such, more difficult to analyze. The launch of the space telescopes *James Webb* (JWST) & *Ariel* will give rise to an explosion in the quality and quantity of spectroscopic data available for an unprecedented number of exoplanets in our galaxy. Accurately extracting the information content, thereby permitting atmospheric science, of such data-sets will require robust models and techniques. We present here the analysis of simulated transmission spectra for water-rich atmospheres, giving evidence for non-negligible differences in simulated transit depths when self-broadening of H_2O is correctly accounted for, compared with the currently typically accepted standard of using H_2 and He-broadened cross-sections. Our case-study analysis is carried out on two super-Earths, focusing on water-based atmospheres, ranging from H_2-rich to H_2O-rich. The transit depth is considerably affected, increasing values by up to 60 ppm, which is shown to be detectable with JWST and Ariel. The differences are most pronounced for the lighter (i.e. $\mu \sim 4$) atmospheres. Our work illustrates that it is imperative that the field of exoplanet spectroscopy moves toward adapted cross-sections, increasingly optimized for high-μ atmospheres for studies of super-Earths and mini-Neptunes.

1. Introduction

The field of exoplanet atmospheric spectroscopy relies heavily upon accurately derived cross-sections, generated for particular pressure and temperature ranges as well as for specific molecules. As the number of known exoplanets continues to increase rapidly, we are witnessing an influx of small, more temperate worlds ($\leq 10\,M_\oplus, \leq 5000$ K). The range of super-Earths and mini-Neptunes discovered has opened up the field of possibilities for observable atmospheres on these planets. Prime examples include the TRAPPIST-1 system, [1], 55 Cnc e [2, 3], GJ 1132 b [4, 5], GJ 1214 b [6], K2-18 b [7] and LHS 1140 b [8].

Small planets of increasing interest in the field are those that lie within the radius valley ([9], [10], [11]), i.e. between $1.5 - 2.0\,R_\oplus$, whereby the dearth of planets in this region is theorized to be consistent with the intersection between super-Earths and sub-Neptunes or water-worlds. Planets smaller than $1.8\,R_\oplus$ could have thinner, possibly H_2-depleted atmospheres (e.g. [12, 13, 14]), whilst planets with radii larger than this threshold could possess volatile-rich atmospheres, H_2/He or H_2O-rich in particular (e.g. [15, 16]). However, observational constraints, in the form of atmospheric transmission spectra, are needed to confirm these hypotheses and therefore the nature of these transitional planets. Furthermore, this population of small planets deviates from our understanding of planet atmospheres which has been mostly built upon our knowledge of hot-Jupiters and the solar system. For example, cross-sections that are utilized in the exoplanet field (based on the line lists provided by ExoMol [17]), HITRAN [18], MoLLIST [19] and HITEMP [20]) are typically generated for atmospheres which are either dominated by H_2 and He, or air for Earth-like planets, in the case of HITRAN (see recent works, such as [21, 22, 23, 24]). Whilst this is appropriate for gas giant planets or Earth-like planets, such cross-sections do not include effects such as the self-broadening of heavy molecules like H_2O. When considering atmospheres heavier than H_2/He, such as is expected to be prevalent on super-Earths and water worlds [16, 25, 26, 27, 28], this provides a non-negligible difference in the simulated (wavelength-dependent) atmospheric signal obtained during transit, knows as the *transit depth*.

H_2 and He are light molecular species which only interact weakly with other molecules at long range and are therefore very inefficient line broadeners. Water, conversely, is both heavier and possesses a significant dipole which leads to enhanced long-range interactions. Broadening by water vapour is known to be significant in the Earth's atmosphere even though it is generally only a trace species. As transit spectroscopy probes regions of an exoplanet atmosphere as it approach optical thickness, the increased line broadening by water can be expected to lead to significantly enhanced overall absorption compared to the case where only H_2 and He are considered.

Previous works have investigated the effects of various choices when computing cross-sections for modelling exoplanet atmospheres, such as [29, 30, 31, 32]. These investigations included the choice of broadening parameters, although these typically focus on H_2/He atmospheres and associated broadening parameters. Recently there has been some work more focused on cross-sections for heavier atmospheres, such as [28, 33].

In this work we investigate the effects of including H_2O self-broadening, in addition to H_2/He-broadening, in the calculation of our water cross-sections which we use to model exoplanet atmospheres. We find that the transit depth is considerably affected; the largest difference being found for one of our case-study planets GJ 1214 b, a 6.26 $M_{\oplus}$, 2.85 $R_{\oplus}$ super-Earth.

2. Methodology

2.1. Transmission spectroscopy

If the orbital plane of a planet around its host star is aligned approximately parallel to our line of sight with the system (analogous to 90° inclination), the planet will transit in front of its star. Assuming that there is no atmosphere and that the planet is totally opaque to its incoming starlight, this transiting motion will cause a drop in the amount of stellar flux we receive from the host star. This change in detected light is known as the *transit depth*, ΔF, which is equal to the ratio between the surface area of the planet (as we view it, in 2D) and the surface area of the star. Since we assume both objects to be totally symmetrical, this reduces to:

$$\Delta F = \frac{F_{out} - F_{in}}{F_{out}} = \left(\frac{R_p}{R_*}\right)^2 \qquad (1)$$

which gives a measure of the relative change in flux as the planet blocks its starlight. This provides us with an observable quantity with which we can

quantify the size of the planet, if we know the stellar properties, which can be derived from models.

Now, if the planet possesses an atmosphere, an envelope of gas which surrounds the planet which is maintained by the planet's gravitational force, the molecules present will absorb, scatter and reflect incoming starlight, in addition to thermally emitting photons. Owing to the varied and distinct spectral characteristics of different molecules, how opaque a certain atmosphere is to incoming stellar flux will vary significantly with wavelength. This information is described by the quantity $\tau(\lambda)$, given in Eq. 2, known as the *optical depth*. Overall, regarding transmission spectroscopy, we can treat the atmosphere as a purely absorbing and single-scattering medium as a good (first-order) approximation for radiative transfer through the planetary atmosphere.

Given an arbitrary path through the atmosphere for which radiation transmits with wavelength-dependent initial intensity I_λ, the transmitted radiance will be attenuated by absorption and scattering processes. We can denote this reduction in intensity as a function of path ds as $dI_\lambda/ds = -I_\lambda \sigma_\lambda \rho$, where σ_λ is the total mass extinction cross section (the sum of the absorption and scattering cross sections) and ρ is the density of the medium. Integrating up and using the fact that the optical depth as a function of atmospheric height is determined by summing the opacity contributions of all molecular species present, we recover the *Beer-Bougert-Lambert Law*:

$$I_\lambda(z) = I_\lambda(0)e^{-\tau_\lambda(z)} \quad \text{with} \quad \tau_\lambda(z) = \sum_m \int_z^{z_\infty} \sigma_{m,\lambda}(z')\chi_m(z')\rho(z')dz', \quad (2)$$

where χ_m and ρ are the column density of a given molecular species and the number density of the atmosphere, respectively.

We may now rewrite Eq. (1) as:

$$\Delta F = \frac{F_{out} - F_{in}}{F_{out}} = \left(\frac{R_p + h_\lambda}{R_*}\right)^2 \approx \frac{R_p^2 + 2R_p h_\lambda}{R_*^2} \qquad O(h_\lambda) \qquad (3)$$

where we may describe the atmospheric height function as:

$$2R_p h_z = 2\int_0^{z_{max}} (R_p + z)(1 - e^{-\tau_\lambda(z)})dz, \qquad (4)$$

where z_{max} denotes the height of the atmosphere.

4

Using this formalism, the transit depth of an atmosphere-bearing planet for any given wavelength may be calculated, using derived *cross-sections* (temperature, pressure and wavelength dependent) for a given molecular species. If we populate a model atmosphere with a given temperature profile, pressure profile, chemical species abundances and a specified cloud distribution we may generate a transmission spectrum (ΔF vs. λ) for the atmosphere, thereby *forward-modelling* it. To date, there is extensive literature pertaining to the collection of transmission data, alongside analysis of the generated transmission spectra, for a wide variety of exoplanets; from hot-Jupiters [34, 35, 36] to habitable-zone super-Earths [1, 7, 8].

2.2. Broadening parameters

The Voigt profile is commonly used to represent line broadening in exoplanet atmospheres, which is a convolution of the temperature-dependent Gaussian line profile and the pressure-dependent (and therefore dependent on broadening species) Lorentzian profile. The equation for the Lorentzian line width (HWHM) for a given pressure P and temperature T, is given by:

$$\gamma_L = \gamma \left(\frac{T_0}{T}\right)^n \frac{P}{P_0}.$$

(5)

Here, T_0 and P_0 are the reference temperature and pressure, whilst γ and n are the reference HWHM and temperature exponent, respectively. The latter two terms are known as pressure-broadening parameters and are dependent primarily on the molecular species being broadened and the species inducing it. Therefore these are the parameters which, upon variation, enable us to study the self-broadening effects of water considered in this study; considering atmospheres comprising varying levels of H_2O with respect to H_2 and He. We note that the power law for temperature dependence which we assume in this work may not work well over large temperature ranges, including those temperatures of the atmospheres we are modeling. This has been demonstrated by works such as [37], who developed the more advanced Gamache–Vispoel double power law (DPL) model. Others, such as Wcisło *et al.* [38] highlight non-Voigt effects to line broadening. We will consider updating our cross-sections using these more robust line-shape models in the future. We also expect to have more robust values for the self-broadening parameters of H_2O and other molecular species, as a result of ongoing work from projects such as ExoMol [39] and HITRAN [40] and others [41, 42],

5

which we would like to incorporate into our cross-sections in the future. For the present study we use the Voigt profile of Eq. 5. The self-broadened H_2O cross-sections used in this study were computed using ExoCross [43], as were the H_2/He-broadened cross-sections for H_2O. The latter are similar to those from the ExoMolOP database [21] but with J-dependent broadening parameters (where J is the rotational angular momentum quantum number) from the ExoMol website[1] used for H_2 and He broadening [44, 45]. All H_2O cross-sections presented here use the ExoMol POKAZATEL line list [46]. We computed the line wings out to 500 Voigt widths in all cases, out to a maximum of 25 cm^{-1}. The values of γ and n for the self-broadening of H_2O used in the present study are detailed below.

2.2.1. Self-broadened half-width, γ_{H_2O}

There are many literature sources with broadening parameters for self-broadening of H_2O. For example, Gamache and Hartmann [47] compiled and compared various parameters related to H_2O line shape, including values for the half-width γ for self-H_2O broadening. There are over 47,000 lines in their database, with values of γ_{H_2O} ranging from 0.108 - 0.805 cm^{-1} atm^{-1}. The 2020 release of the HITRAN database [48], who follow a "diet" procedure [49], provide an update of this 2004 broadening measurement database of [47]. A simple average of all values of the main isotopologue of H_2O (with no weighting) from HITRAN2020 for γ_{H_2O} yields a value of 0.35 cm^{-1} atm^{-1}. There are many other works with available broadening values: for example, [50] and [51] both present a number of values for γ_{H_2O} for a few thousand lines each. They report average values of $\gamma_{H_2O} = 0.4$ and between 0.1 and 0.5 cm^{-1} atm^{-1}, respectively.

As noted above, for the present study we extract the broadening parameters from the HITRAN2020 [48] database as a function of rotational angular momentum quantum number J, computing an average value of γ for each value of J. The data extends up to a maximum of J=26 and varies between 0.1 cm^{-1} atm^{-1} for high J to 0.5 cm^{-1} atm^{-1} for low J.

2.2.2. Temperature exponent n_{H_2O} for self-broadened half-width

HITRAN2020 [48] currently only include γ_{self} and not n_{self} values for H_2O, due to the large effort required to validate and populate such parameters

---

[1]https://www.exomol.com/data/data-types/broadening_coefficients/H2O/

into their database. For now we use averaged J-dependent values for γ_{self} from HITRAN2020 [48] and an apparently typical value of $n_{\text{self}}=0.7$ for H_2O. The focus of some ongoing and future work is to update the ExoMol [39] and ExoMolOP [21] databases to include broadening parameters in a more comprehensive way. This is not a simple undertaking: the H_2O line list used in this work, for example, ExoMol POKAZATEL [46], contains 6 billion transitions between 800,000 energy levels, with even larger line lists required to describe larger species, see Table 13 of [21].

Although it is beyond the scope of the current study to perform a comprehensive assessment of available temperature exponents for self-broadening of H_2O, there are a number of studies in the literature which have focused on analysing water vapor spectra at various temperatures in order to determine the temperature dependence n of the self-broadened half-width γ. Here, we summarize the results from a selection of works, but note that this is not a comprehensive sample. Grossmann and Browell [52] analyzed spectra of water vapor in the 720 nm region, finding an average value of $n=0.75$. Studies such as [53, 54, 55] all analyzed particular rotational lines in the low-wavenumber region of the spectra, between around 250 - 390 K. They find values of n_{self} of 0.62, 0.89 and 0.85, respectively. Both [54, 55] look at various broadeners, including self. They find that both γ and n are generally larger for the cases where H_2O is the broadener, in comparison to N_2, O_2 or Ar as broadeners (n is 0.52, 0.64, 0.49 for those cases, respectively for example in [54]). Alder-Golden *et al.* [56] analyzed low-J lines of H_2O close to 12,200 cm^{-1} in the 330 - 540 K temperature range. They find an average value of γ_{self} at 296 K of 0.456 cm^{-1} atm^{-1} (compared to 0.095 cm^{-1} atm^{-1} for air-broadening). The temperature coefficient n for self-broadening of H_2O was found to be 0.9 on average across the spectral region measured. Podobedov *et al.* [57] analyzed several lines of H_2O in the region around 12 - 52 cm^{-1} for temperatures between 263 - 340 K and over a pressure range from 0.0003 - 0.014 bar. The J- and T-dependent values of γ were found to vary between 0.67 - 1.07 cm^{-1} atm^{-1}. They found J-dependent values of n_{self} between 0.56 and 0.81.

Table 2 gives some average values extracted from the HITRAN 2020 [48] database for various molecules and broadeners. The H_2- and He-broadened average values used in the ExoMolOP database [21] (a database tailored for modelling "hot Jupiter"-type exoplanet atmospheres) are also included for reference. It can be seen that in general that the largest γ and n values occur when H_2O is the broadener, which for γ_{H_2O} is an order or magni-
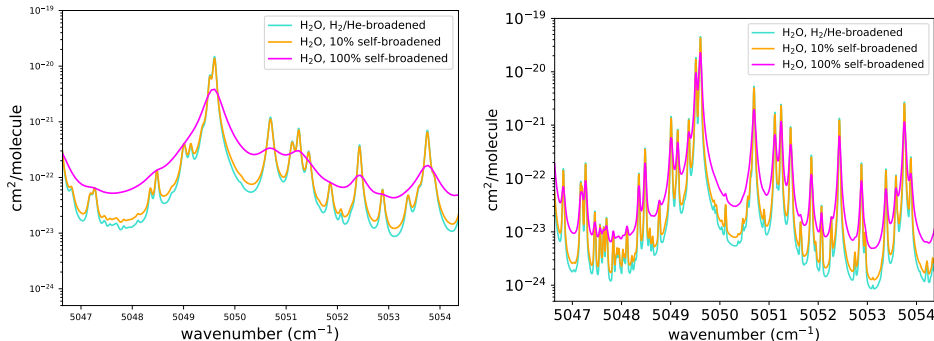
Figure 1: Cross-sections computed using the self-broadening parameters for H_2O, for the abundances of water vapor given in the legend. We compare the self-broadened cross-sections (orange, pink) with the H_2/He-only broadened cross-sections (blue). Left: atmospheric pressure of 1 bar and right: atmospheric pressure of 10^{-1} bar. In an atmosphere with 10% H_2O, we assume the remaining 90% atmosphere is comprized of H_2/He in solar abundances and that the broadening is therefore 90% dominated by H_2/He and the remaining 10% from H_2O self-broadening. In this case we create a combined cross-section which includes 90% of the self-broadened and 10% of the H2/He-broadened cross-section for a given pressure and temperature.

tude larger than H_2- and He-broadening. The contrast between H_2- or He-broadening and H_2O-broadening, however, does not appear to be so large for other species as for water vapor. A similar observation was noted by Gharib-Nezhad and Line [28], who highlight that self-broadening for H_2O is typically up to 7 times larger than H_2/He broadening based on their compilation of literature values.

In Figure 1 we present our derived H_2O-broadened cross-sections at $T = 600$ K for various pressures, in comparison to the standard H_2/He-broadened ones; in both cases it is clear that H_2O self-broadening widens the profiles of each absorption peak.

2.3. Simulating transmission spectra

Eq. (5) exhibits a linear relationship for γ_L with atmospheric pressure, P. Hence, we anticipate the strongest broadening effect to contribute deeper in the atmospheres we wish to model. Consequently, the abundance of water vapor in the atmosphere should affect our results, since although a decrease in molecule number density ought to minimize the overall opacity contribution induced by self-broadening, lighter atmospheres with low-mean-molecular weight allow us to probe deeper pressures; this is illustrated in Figure 2, where
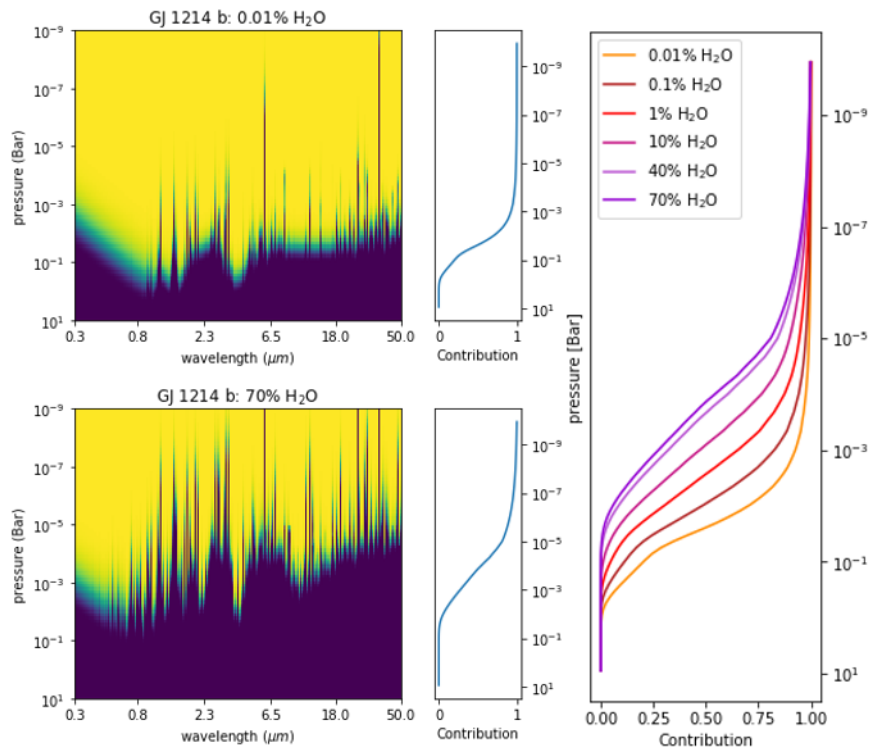
Figure 2: The contribution function, $\frac{d\tau}{dP}$, is defined as the wavelength-averaged variation in the optical depth, τ with pressure, P. On the LHS, τ is plotted in $\mu - P$ space; for which the contribution $\frac{d\tau}{dP}$ is normalized and displayed in the central panel; whilst on the RHS this contribution is plotted for varying water vapor abundance; illustrating that deeper pressures can be probed in lighter atmospheres.

the contribution function, $\frac{d\tau}{dP}$, is defined as the wavelength-averaged variation in the optical depth, τ with pressure, P. This informs our implementation of atmospheric models endowed with a variety of water vapor abundances, in order to examine for which abundances the self-broadening effects of H_2O are both most prominent and most observable with future space missions.

In order to simulate forward models of transmission spectra for GJ 1132 b and GJ 1214 b, this analysis was performed using the publicly available retrieval suite TauREx 3.0 [58, 59, 60]. For the stellar parameters and the planet mass, we used the values from [61] and [62] as given in Table 1 a). In our runs we assumed that the planets possess a range of different water-based atmospheres, with fill gas abundance ratio given by $V_{H_2O} = x$, with

9

Table 1: a) stellar and planetary parameters for two small planets, for input into TauREx 3.0, derived from [61], [62], b) list of the forward-modeled parameters, their values and the scaling used.

a) stellar & planetary parameters		
parameter	GJ 1132 b	GJ 1214 b
T_* [K]	3270	3026
R_* [$R_\odot$]	0.207	0.220
M_* [$M_\odot$]	0.181	0.176
M_p [$M_\oplus$]	1.66	6.26
R_p [$R_\oplus$]	1.13	2.85
$P_{orbital}$ [days]	1.63	1.58

b) forward model parameters			
parameter	GJ 1132 b	GJ 1214 b	type
P_{clouds}	None	None	opaque
T [K]	500	600	iso.
$\log_{10} V_{H_2O} \in$	[-2, 2]	[-2, 2]	fill
V_{He}	$1e-7$	$1e-7$	trace

the chosen values of x given in Table 1 b) and the remainder of the molecular abundance made up of H_2 and He, as specified. Additionally, we included the collision induced absorption (CIA) from H_2-H_2 [63, 64] and H_2-He [65], as well as Rayleigh scattering for all molecules. Finally, our simulated atmospheres are cloud-free, isothermal and have molecular abundance profiles which are constant with altitude. The assumptions of isothermal and isochemical atmospheres hold for interpreting current data ([8, 66]). While these approximations might be too simplistic to interpret accurately JWST and Ariel data ([67, 68]), they will not change the conclusions of our paper. For each of the two planets, two types of spectra were generated: one using the standard H_2/He-broadened cross-sections only and another with the H_2O self-broadened cross-sections included for the various percentages of H_2O modeled in the atmosphere, as described in Section 2.2 and illustrated in Figure 1.

3. Results

3.1. Forward-modelling of transmission spectra

We generate transmission spectra at a native resolution of 15,000 for both planets, before binning down to a nominal resolution and signal-to-noise ratio of 200 and 10, respectively, with TauREx 3.0 (enabling eventual comparison with Ariel and JWST errorbars). We utilize both the H_2/He- and the H_2O-broadened cross-sections described in Section 2.1, yielding the spectra given in Figure 3, with planetary and stellar parameters described in detail in Table 1. In comparison with spectra produced using H_2/He-broadened cross-sections, it is evident that by using cross-sections calculated for the water-dominated atmospheres the spectral features are amplified due to the additional absorption achieved by including self-broadening of H_2O. In order to quantify these wavelength-dependent differences, these sets of spectra which are over-plotted the top panels of Figure 3 have been subtracted to obtain the results presented in the lower panels, from which we determine maximum absolute differences in transit depth for the lightest secondary-type atmospheres (10% H_2O); of 60 and 20 ppm for GJ 1214 b and GJ 1132 b, respectively.

3.2. Ariel & JWST error-bars

During its primary mission, Ariel will survey the atmospheres of 1000 exoplanets [69, 70] and many of these targets could be in the Super-Earth and Sub-Neptune regime [71]. Meanwhile, during the Guaranteed Time Observations (GTO) and first cycle of the General Observing (GO), around 70 planets will be observed with JWST [72]. Nearly half of these JWST targets have a radius of $\leq 2.5 R_\oplus$ and, therefore, may not have a H_2-dominated atmosphere. During its lifetime, JWST is expected to observe a couple of hundred exoplanets [e.g. 73].

To investigate the detectability of broadening-induced differences with future instruments, we generated error bars for the simulated spectra. We then compared the size of these uncertainties to the absolute differences between the H_2- and H_2O-broadened spectra. For Ariel, we generated error bars using ArielRad [74] while, for JWST, we used a modified version of the radiometric tool described in Edwards and Stotesbury [75] which utilizes the JWST instrument parameters from Pandeia [76].

For JWST we modeled observations with NIRISS GR700XD (0.8 - 2.8 μm) and NIRSpec G395M (2.9 - 5.3 μm), whilst for Ariel, which provides
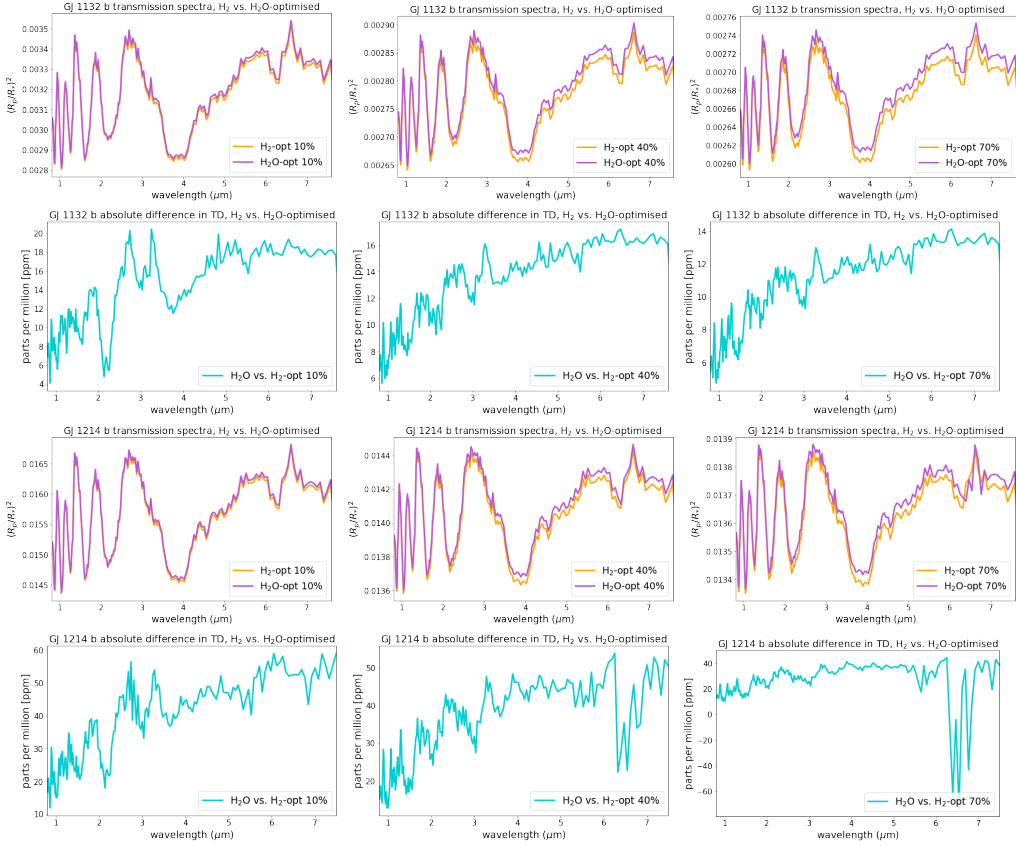
Figure 3: Individual over-plots of the (resolution 200) spectra produced with both H_2 and H_2O-broadened cross-sections for each planet, for varying water abundance, with absolute differences beneath. Top: GJ 1132 b (500 K), bottom: GJ 1214 b (600 K).

simultaneous coverage from 0.5 - 7.8 μm, we simulated error bars at tier 2 resolution. Presented in Figure 4, for GJ 1132 b and GJ 1214 b, we observe that both instruments will be sensitive enough to reveal such differences when integrating multiple transits, specifically 45 and 40 in the case of Ariel (tier 2) and 10 and 5 in the case of JWST for GJ 1132 b and GJ 1214 b, respectively. We note that both these planets will be studied by JWST in the first cycle of observations.
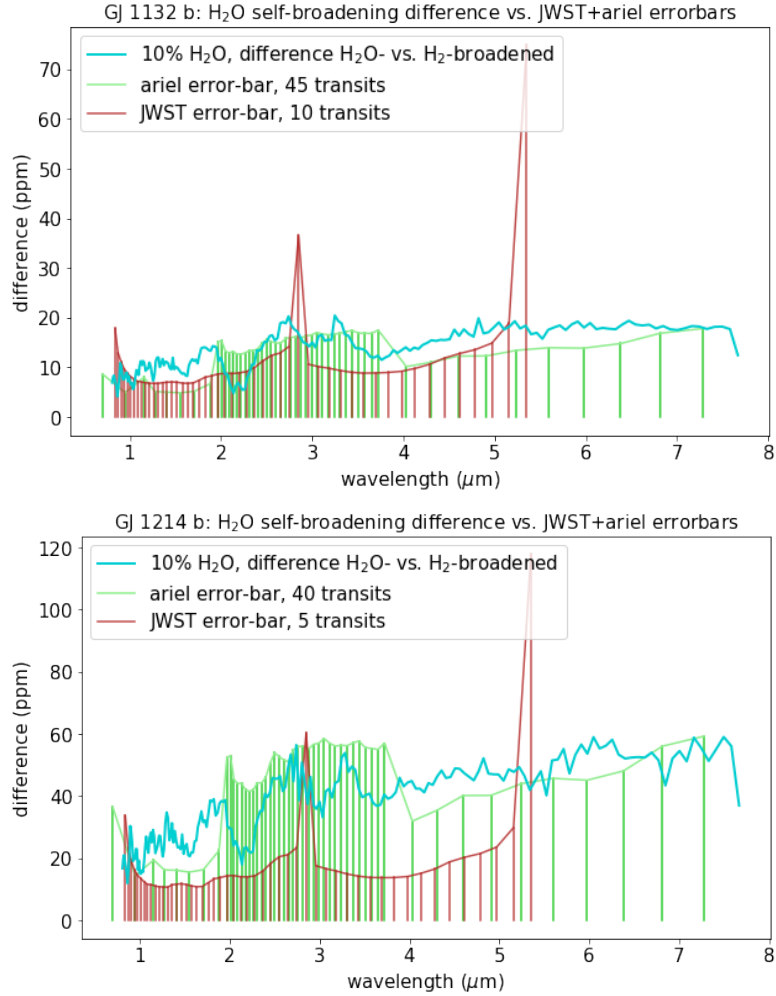
Figure 4: Comparison of simulated error bars for observation of a) GJ 1132 b and b) GJ 1214 b with future-missions Ariel and JWST with the absolute wavelength-dependent differences in transit depth on the simulated transmission spectra, using H_2- vs. H_2O-broadened cross-sections. In both cases these broadening-induced differences should be directly observable in the near-future.

13

4. Discussion

In all spectra, an increase in μ, corresponding to increased volume mixing ratio of water, corresponds to reduced scale height, since $H = \frac{kT}{\mu g}$, (where μ is the mean molecular weight of the atmosphere, g is the planet gravity and k is the Boltzmann constant). For the individual atmospheres we observe a saturation of features as the atmospheric mean-molecular-weight gets larger. In tandem, an increase in mean-molecular weight of the atmosphere results in a decrease in the atmospheric pressure at which we can probe, as illustrated in Figure 2. Thus, the largest observed differences in transit depth vs. wavelength are found in the lightest secondary-type atmospheres, namely those with 10% water vapor, for all employed temperatures. As for the two planets considered, the largest transit depth increases are observed in GJ 1214 b, with an equilibrium temperature of 600 K, as opposed to HAT-P-11 b, which possesses an equilibrium temperature of 900 K.

Although the Lorentzian line profile for H_2O self-broadening is approximately inversely proportional to the atmospheric temperature, low-temperature planets have smaller global transit depths, due to the reduction in scale height the temperature induces. Hence, there is a trade-off between the strength of the broadening effect and detectability of such effects. Our work finds that the atmospheric temperatures for such differences to become detectable with future missions, as discussed, is thus ~ 600 K.

Thus, consideration and utilization of self-broadening effects induced by not just H_2O, but all large-μ molecules should have a stronger impact on the medium-cool atmospheres of temperate planets, as well as those with low-mean-molecular-weight secondary atmospheres, namely those closer to the threshold abundance of around 10% non-H_2 or -He which we define to the boundary between primary and secondary type atmospheres; precisely those planets which sit in the transition region between super-Earths and sub-Neptunes, whose atmospheres remain illusive and out-of-reach with current telescopes, due to known limits on both the signal-to-noise and resolution ([8]. The next generation of telescopes will widen and deepen our spectral view, both in terms of signal-to-noise and resolution, but also in wavelength coverage; hence these problems should be easily tackled with Ariel and JWST. It is therefore especially imperative for the accuracy of cross-section data to compete with the level of precision obtainable with these future facilities.

Standard H_2/He-broadened cross-sections which are in widespread use by the exoplanet community are simply non-optimal for the study of secondary-type, heavy atmospheres dominated by non-H_2/He species due to the fact that these opacities are calculated with respect to a nominal atmosphere which is dominated by H_2 and He. At present, due to the computationally-intensive nature of numerically evaluating absorption strengths for molecular transitions and interactions for a given atmospheric species, specifying a grid of temperature and pressure values is necessary to obtain computable opacities for input into forward models and atmospheric retrieval algorithms. It is well known that extrapolating opacities above the temperature or pressure grid on which they were computed can be problematic (e.g. [77], [78]), largely due to the dominance of transitions that originate in energy levels above the ground-state in higher temperature regimes. In this work we demonstrate that including self-broadening effects into the calculation of the absorption cross-section of water markedly affects the simulated transit depth of small-planet exoplanet atmospheres. Moreover, we are the first in the exoplanet field to illustrate that these generated differences are detectable with the near-future space missions JWST & Ariel, by explicitly simulating spectra with error bars for these instruments. We prove that self-broadening is necessary to account for in these calculations. As a community, our long-term goal should be to develop cross-section functions, explicitly derived for pressure-temperature grids and as a function of molecular abundances, with all intra- and inter-molecular effects, like self-broadening, included.

5. Conclusion

In summary, it is evident that accounting for previously thought-to-be negligible absorption contributions, such as the self-broadening exhibited by H_2O in our opacity functions, will alter simulated transit depths by as much as 60 ppm. These differences sit above the noise level for a reasonable number of transit observations with the near-future space telescopes JWST and Ariel for the two small planets considered: GJ 1132 b and GJ 1214 b. Our quantification of the transit depth differences found by producing and utilising cross-sections which include the absorption contribution induced by H_2O self-broadening motivate further progress in not only refining such broadening parameters, but also developing opacities for a variety of molecular species expected to be found in the atmospheres of small planets, which may also be dominated by more than one heavy molecule. This is not an easy

15

undertaking, due to the vast amount of work done and ongoing in the field of line shapes (including half widths γ_{H_2O} and temperature dependence n_{H_2O}; see, for example, [47, 40, 48, 50] and references therein). It is paramount that the field of exoplanet spectroscopy moves towards the use of more adaptive cross-sections, built as functions not only of temperature and pressure but also of molecular abundance, as we have illustrated specifically for the case of H_2O.

6. Acknowledgements

References

[1] J. de Wit, H. R. Wakeford, N. K. Lewis, et al., Atmospheric reconnaissance of the habitable-zone earth-sized planets orbiting trappist-1, Nature Astronomy 2 (2018) 214–219. URL: `http://dx.doi.org/10.1038/s41550-017-0374-z`. doi:`10.1038/s41550-017-0374-z`.

[2] A. Tsiaras, M. Rocchetto, I. P. Waldmann, et al., Detection of an Atmosphere Around the Super-Earth 55 Cancri e, ApJ 820 (2016) 99. doi:`10.3847/0004-637X/820/2/99`. arXiv:`1511.08901`.

[3] B.-O. Demory, M. Gillon, J. de Wit, N. Madhusudhan, et al., A map of the large day–night temperature gradient of a super-earth exoplanet, Nature 532 (2016) 207–209. URL: `http://dx.doi.org/10.1038/nature17169`. doi:`10.1038/nature17169`.

[4] J. E. Libby-Roberts, Z. K. Berta-Thompson, H. Diamond-Lowe, et al., The Featureless HST/WFC3 Transmission Spectrum of the Rocky Exoplanet GJ 1132b: No Evidence For A Cloud-Free Primordial Atmosphere and Constraints on Starspot Contamination, arXiv e-prints (2021) arXiv:2105.10487. arXiv:`2105.10487`.

[5] L. V. Mugnai, D. Modirrousta-Galian, B. Edwards, Q. Changeat, et al., ARES V: No Evidence For Molecular Absorption in the HST WFC3 Spectrum of GJ 1132 b, arXiv e-prints (2021) arXiv:2104.01873. `arXiv:2104.01873`.

[6] L. Kreidberg, J. L. Bean, J.-M. Désert, B. Benneke, D. Deming, K. B. Stevenson, S. Seager, Z. Berta-Thompson, A. Seifahrt, D. Homeier, Clouds in the atmosphere of the super-Earth exoplanet GJ1214b, Nature 505 (2014) 69–72. doi:`10.1038/nature12888`. `arXiv:1401.0022`.

[7] A. Tsiaras, I. P. Waldmann, G. Tinetti, J. Tennyson, S. N. Yurchenko, Water vapour in the atmosphere of the habitable-zone eight-earth-mass planet k2-18 b, Nature Astronomy (2019). URL: `http://dx.doi.org/10.1038/s41550-019-0878-9`. doi:`10.1038/s41550-019-0878-9`.

[8] B. Edwards, Q. Changeat, M. Mori, L. O. Anisman, et al., Hubble wfc3 spectroscopy of the habitable-zone super-earth lhs 1140 b, The Astronomical Journal 161 (2020) 44. URL: `http://dx.doi.org/10.3847/1538-3881/abc6a5`. doi:`10.3847/1538-3881/abc6a5`.

[9] J. E. Owen, Y. Wu, The Evaporation Valley in the Kepler Planets, ApJ 847 (2017) 29. doi:`10.3847/1538-4357/aa890a`. `arXiv:1705.10810`.

[10] B. J. Fulton, E. A. Petigura, The California Kepler Survey VII. Precise Planet Radii Leveraging Gaia DR2 Reveal the Stellar Mass Dependence of the Planet Radius Gap, ArXiv e-prints (2018). `arXiv:1805.01453`.

[11] V. Van Eylen, C. Agentoft, M. S. Lundkvist, H. Kjeldsen, J. E. Owen, B. J. Fulton, E. Petigura, I. Snellen, An asteroseismic view of the radius valley: stripped cores, not born rocky, Monthly Notices of the Royal Astronomical Society 479 (2018) 4786–4795. URL: `http://dx.doi.org/10.1093/mnras/sty1783`. doi:`10.1093/mnras/sty1783`.

[12] D. Valencia, M. Ikoma, T. Guillot, N. Nettelmann, Composition and fate of short-period super-earths, Astronomy and Astrophysics 516 (2010) A20. URL: `http://dx.doi.org/10.1051/0004-6361/200912839`. doi:`10.1051/0004-6361/200912839`.

[13] J. Leconte, F. Forget, H. Lammer, On the (anticipated) diversity of terrestrial planet atmospheres, Experimental Astronomy 40 (2015) 449–467. URL: `https://doi.org/10.1007/s10686-014-9403-4`.

[14] C. D. Dressing, D. Charbonneau, X. Dumusque, et al., The Mass of Kepler-93b and The Composition of Terrestrial Planets, ApJ 800 (2015) 135. doi:`10.1088/0004-637X/800/2/135`. `arXiv:1412.8687`.

[15] D. Valencia, T. Guillot, V. Parmentier, R. S. Freedman, Bulk composition of gj 1214b and other sub-neptune exoplanets, The Astrophysical Journal 775 (2013) 10. URL: `http://dx.doi.org/10.1088/0004-637X/775/1/10`. doi:`10.1088/0004-637x/775/1/10`.

[16] L. Zeng, S. B. Jacobsen, D. D. Sasselov, et al., Growth model interpretation of planet size distribution, Proceedings of the National Academy of Sciences 116 (2019) 9723–9728. doi:`10.1073/pnas.1812905116`.

[17] J. Tennyson, S. N. Yurchenko, A. F. Al-Refaie, et al., The exomol database: Molecular line lists for exoplanet and other hot atmospheres, Journal of Molecular Spectroscopy 327 (2016) 73 – 94. doi:`https://doi.org/10.1016/j.jms.2016.05.002`, new Visions of Spectroscopic Databases, Volume II.

[18] I. Gordon, L. S. Rothman, J. S. Wilzewski, R. V. Kochanov, C. Hill, Y. Tan, P. Wcislo, HITRAN2016 : new and improved data and tools towards studies of planetary atmospheres, in: AAS/Division for Planetary Sciences Meeting Abstracts #48, volume 48 of *AAS/Division for Planetary Sciences Meeting Abstracts*, 2016, p. 421.13.

[19] P. F. Bernath, MoLLIST: Molecular line lists, intensities and spectra, J. Quant. Spectrosc. Radiat. Transf. 240 (2020) 106687. doi:`10.1016/j.jqsrt.2019.106687`.

[20] L. S. Rothman, I. E. Gordon, R. J. Barber, et al., HITEMP, the High-Temperature Molecular Spectroscopic Database, J. Quant. Spectrosc. Radiat. Transf. 111 (2010) 2139–2150. doi:`10.1016/j.jqsrt.2010.05.001`.

[21] K. L. Chubb, M. Rocchetto, A. F. Al-Refaie, I. Waldmann, M. Min, J. Barstow, P. Molliére, M. W. Phillips, J. Tennyson, S. N. Yurchenko, The ExoMolOP Database: Cross-sections and k-tables for molecules of interest in high-temperature exoplanet atmospheres, A&A 646 (2020) A21.

[22] D. Kitzmann, K. Heng, M. Oreshenko, S. L. Grimm, D. Apai, B. P. Bowler, A. J. Burgasser, M. S. Marley, Helios-r2: A new bayesian, open-source retrieval model for brown dwarfs and exoplanet atmospheres, ApJ 890 (2020) 174. doi:10.3847/1538-4357/ab6d71.

[23] M. W. Phillips, P. Tremblin, I. Baraffe, G. Chabrier, N. F. Allard, F. Spiegelman, J. M. Goyal, B. Drummond, E. Hebrard, A new set of atmosphere and evolution models for cool t-y brown dwarfs and giant exoplanets, A&A 637 (2020) A38. doi:10.1051/0004-6361/201937381.

[24] S. L. Grimm, M. Malik, D. Kitzmann, et al., HELIOS-K 2.0 and an Open-source Opacity Database for Exoplanetary Atmospheres, The Astrophysical Journal Supplement 253 (2021) 30. doi:10.3847/1538-4365/abd773.

[25] E. Ducrot, M. Gillon, L. Delrez, et al., Trappist-1: Global results of the spitzer exploration science program red worlds, Astronomy & Astrophysics 640 (2020) A112. URL: http://dx.doi.org/10.1051/0004-6361/201937392. doi:10.1051/0004-6361/201937392.

[26] I. J. M. Crossfield, D. Dragomir, N. B. Cowan, T. Daylan, I. Wong, T. Kataria, D. Deming, L. Kreidberg, T. Mikal-Evans, V. Gorjian, et al., Phase curves of hot neptune ltt 9779b suggest a high-metallicity atmosphere, The Astrophysical Journal 903 (2020) L7. URL: http://dx.doi.org/10.3847/2041-8213/abbc71. doi:10.3847/2041-8213/abbc71.

[27] F. Wunderlich, M. Scheucher, M. Godolt, J. L. Grenfell, et al., Distinguishing between wet and dry atmospheres of trappist-1 e and f, The Astrophysical Journal 901 (2020) 126. URL: http://dx.doi.org/10.3847/1538-4357/aba59c. doi:10.3847/1538-4357/aba59c.

[28] E. Gharib-Nezhad, M. R. Line, The influence of H_2O pressure broadening in high-metallicity exoplanet atmospheres, Astrophys. J. 872 (2019) 27. doi:10.3847/1538-4357/aafb7b.

[29] C. Hedges, N. Madhusudhan, Effect of pressure broadening on molecular absorption cross sections in exoplanetary atmospheres, Mon. Not. R. Astron. Soc. 458 (2016) 1427–1449. doi:10.1093/mnras/stw278.

[30] M. Rocchetto, Characterisation of Exoplanetary Atmospheres and Planetary Systems, Ph.D. thesis, University College London, London, UK, 2017.

[31] J. K. Barstow, Q. Changeat, R. Garland, M. R. Line, M. Rocchetto, I. P. Waldmann, A comparison of exoplanet spectroscopic retrieval tools, Mon. Not. R. Astron. Soc. (2020). doi:`10.1093/mnras/staa548`.

[32] E. Gharib-Nezhad, A. R. Iyer, M. R. Line, R. S. Freedman, M. S. Marley, N. E. Batalha, EXOPLINES: Molecular absorption cross-section database for brown dwarf and giant exoplanet atmospheres, The Astrophysical Journal Supplement Series 254 (2021) 34. doi:`10.3847/1538-4365/abf504`.

[33] L. O. Anisman, K. L. Chubb, J. Elsey, A. Al-Refaie, Q. Changeat, S. N. Yurchenko, J. Tennyson, G. Tinetti, Cross-sections for heavy atmospheres: H2o continuum, Journal of Quantitative Spectroscopy and Radiative Transfer 278 (2022) 108013. doi:`https://doi.org/10.1016/j.jqsrt.2021.108013`.

[34] N. Skaf, M. F. Bieger, B. Edwards, Q. Changeat, M. Morvan, F. Kiefer, D. Blain, T. Zingales, M. Poveda, A. Al-Refaie, et al., Ares. ii. characterizing the hot jupiters wasp-127 b, wasp-79 b, and wasp-62b with the hubble space telescope, The Astronomical Journal 160 (2020) 109. URL: `http://dx.doi.org/10.3847/1538-3881/ab94a3`. doi:`10.3847/1538-3881/ab94a3`.

[35] A. Pinhas, N. Madhusudhan, S. Gandhi, R. MacDonald, H2o abundances and cloud properties in ten hot giant exoplanets, Monthly Notices of the Royal Astronomical Society 482 (2019) 1485–1498. doi:`10.1093/mnras/sty2544`.

[36] D. K. Sing, J. J. Fortney, N. Nikolov, et al., A continuum from clear to cloudy hot-jupiter exoplanets without primordial water depletion, Nature 529 (2015) 59–62. URL: `http://dx.doi.org/10.1038/nature16068`. doi:`10.1038/nature16068`.

[37] R. R. Gamache, B. Vispoel, On the temperature dependence of half-widths and line shifts for molecular transitions in the microwave and

infrared regions, JQSRT 217 (2018) 440–452. doi:`10.1016/j.jqsrt.2018.05.019`.

[38] P. Wcisło, I. E. Gordon, H. Tran, et al., The implementation of non-voigt line profiles in the HITRAN database: H_2 case study, J. Quant. Spectrosc. Radiat. Transf. 177 (2016) 75 – 91. doi:`10.1016/j.jqsrt.2016.01.024`, xVIIIth Symposium on High Resolution Molecular Spectroscopy (HighRus-2015), Tomsk, Russia.

[39] J. Tennyson, S. N. Yurchenko, A. F. Al-Refaie, V. H. Clark, K. L. Chubb, et al., The 2020 release of the exomol database: Molecular line lists for exoplanet and other hot atmospheres, Journal of Quantitative Spectroscopy and Radiative Transfer 255 (2020) 107228. doi:`0.1016/j.jqsrt.2020.107228`.

[40] Y. Tan, R. V. Kochanov, L. S. Rothman, I. E. Gordon, Introduction of water-vapor broadening parameters and their temperature-dependent exponents into the HITRAN database: Part I—CO2, N2O, CO, CH4, O2, NH3, and H2S, Journal of Geophysical Research: Atmospheres 124 (2019) 11580–11594. doi:`10.1029/2019JD030929`.

[41] J.-M. Hartmann, H. Tran, R. Armante, C. Boulet, A. Campargue, F. Forget, L. Gianfrani, I. Gordon, S. Guerlet, M. Gustafsson, J. T. Hodges, S. Kassi, D. Lisak, F. Thibault, G. C. Toon, Recent advances in collisional effects on spectra of molecular gases and their practical consequences, J. Quant. Spectrosc. Radiat. Transf. 213 (2018) 178 – 227. doi:`10.1016/j.jqsrt.2018.03.016`.

[42] N. Stolarczyk, F. Thibault, H. Cybulski, H. Jóźwiak, G. Kowzan, B. Vispoel, I. Gordon, L. Rothman, R. Gamache, P. Wcisło, Evaluation of different parameterizations of temperature dependences of the line-shape parameters based on ab initio calculations: Case study for the hitran database, J. Quant. Spectrosc. Radiat. Transf. 240 (2020) 106676. doi:`10.1016/j.jqsrt.2019.106676`.

[43] S. N. Yurchenko, A. F. Al-Refaie, J. Tennyson, EXOCROSS: a general program for generating spectra from molecular line lists, A&A 614 (2018) A131. doi:`10.1051/0004-6361/201732531`.

[44] E. J. Barton, C. Hill, S. N. Yurchenko, J. Tennyson, A. Dudaryonok, N. N. Lavrentieva, Pressure dependent water absorption cross sections for exoplanets and hot other atmospheres, J. Quant. Spectrosc. Radiat. Transf. 187 (2017) 453–460. doi:10.1016/j.jqsrt.2016.10.024.

[45] E. J. Barton, C. Hill, M. Czurylo, H.-Y. Li, A. Hyslop, S. N. Yurchenko, J. Tennyson, The ExoMol diet of line-by-line pressure-broadening parameters, J. Quant. Spectrosc. Radiat. Transf. 203 (2017) 490–495. doi:10.1016/j.jqsrt.2017.01.028.

[46] O. L. Polyansky, A. A. Kyuberis, N. F. Zobov, J. Tennyson, S. N. Yurchenko, L. Lodi, Exomol molecular line lists xxx: a complete high-accuracy line list for water, Monthly Notices of the Royal Astronomical Society 480 (2018) 2597–2608.

[47] R. R. Gamache, J.-M. Hartmann, An intercomparison of measured pressure-broadening and pressure-shifting parameters of water vapor, Canadian Journal of Chemistry 82 (2004) 1013 – 1027.

[48] I. E. Gordon, L. S. Rothman, R. Hargreaves, et al., The hitran2020 molecular spectroscopic database, JQSRT (2021) 107949. doi:10.1016/j.jqsrt.2021.107949.

[49] I. E. Gordon, L. S. Rothman, R. R. Gamache, et al., Current updates of the water-vapor line list in hitran: A new "diet" for air-broadened half-widths, JQSRT 108 (2007) 389–402. doi:10.1016/j.jqsrt.2007.06.009.

[50] R. A. Toth, Measurements and analysis (using empirical functions for widths) of air- and self-broadening parameters of H_2O, JQSRT 94 (2005) 1–50. doi:10.1016/j.jqsrt.2004.08.041.

[51] J. Loos, M. Birk, G. Wagner, Measurement of positions, intensities and self-broadening line shape parameters of h_2o lines in the spectral ranges 1850-2280 cm^{-1} and 2390-4000 cm^{-1}, JQSRT 203 (2017) 119–132. doi:10.1016/j.jqsrt.2017.02.013.

[52] B. E. Grossmann, E. V. Browell, Spectroscopy of water vapor in the 720-nm wavelength region: Line strengths, self-induced pressure broadenings and shifts, and temperature dependence of linewidths

and shifts, Journal of Molecular Spectroscopy 136 (1989) 264–294. doi:10.1016/0022-2852(89)90336-6.

[53] V. Markov, Temperature dependence of self-induced pressure broadening and shift of the 643-550 line of the water molecule, Journal of Molecular Spectroscopy 164 (1994) 233–238. doi:10.1006/jmsp.1994.1069.

[54] A. Bauer, M. Godon, M. Kheddar, J. Hartmann, J. Bonamy, D. Robert, Temperature and perturber dependences of water-vapor 380 ghz-line broadening, Journal of Quantitative Spectroscopy and Radiative Transfer 37 (1987) 531–539. doi:10.1016/0022-4073(87)90056-2.

[55] A. Bauer, M. Godon, M. Kheddar, J. Hartmann, Temperature and perturber dependences of water vapor line-broadening. experiments at 183 ghz; calculations below 1000 ghz, JQSRT 41 (1989) 49–54. doi:10.1016/0022-4073(89)90020-4.

[56] S. Adler-Golden, J. Lee, N. Goldstein, Diode laser measurements of temperature-dependent line parameters for water vapor near 820 nm, JQSRT 48 (1992) 527–535. doi:10.1016/0022-4073(92)90118-N, special Issue Conference on Molecular Spectroscopic Databases.

[57] V. Podobedov, D. Plusquellic, G. Fraser, Thz laser study of self-pressure and temperature broadening and shifts of water vapor lines for pressures up to 1.4kpa, JQSRT 87 (2004) 377–385. doi:10.1016/j.jqsrt.2004.03.001.

[58] I. P. Waldmann, M. Rocchetto, G. Tinetti, E. J. Barton, S. N. Yurchenko, J. Tennyson, Tau-REx II: Retrieval of Emission Spectra, ApJ 813 (2015) 13. doi:10.1088/0004-637X/813/1/13. arXiv:1508.07591.

[59] I. P. Waldmann, G. Tinetti, M. Rocchetto, E. J. Barton, S. N. Yurchenko, J. Tennyson, Tau-REx I: A Next Generation Retrieval Code for Exoplanetary Atmospheres, ApJ 802 (2015) 107. doi:10.1088/0004-637X/802/2/107. arXiv:1409.2312.

[60] A. F. Al-Refaie, Q. Changeat, I. P. Waldmann, G. Tinetti, TauREx III: A fast, dynamic and extendable framework for retrievals, arXiv e-prints (2019) arXiv:1912.07759. arXiv:1912.07759.

[61] X. Bonfils, J.-M. Almenara, R. Cloutier, A. Wünsche, et al., Radial velocity follow-up of gj1132 with harps, Astronomy & Astrophysics 618 (2018) A142. URL: `http://dx.doi.org/10.1051/0004-6361/201731884`. doi:`10.1051/0004-6361/201731884`.

[62] K. B. W. Harpsøe, S. Hardis, T. C. Hinse, U. G. Jørgensen, et al., The transiting system GJ1214: high-precision defocused transit observations and a search for evidence of transit timing variation, A&A 549 (2013) A10. doi:`10.1051/0004-6361/201219996`. `arXiv:1207.3064`.

[63] M. Abel, L. Frommhold, X. Li, K. L. Hunt, Collision-induced absorption by h2 pairs: From hundreds to thousands of kelvin, The Journal of Physical Chemistry A 115 (2011) 6805–6812.

[64] L. N. Fletcher, M. Gustafsson, G. S. Orton, Hydrogen dimers in giant-planet infrared spectra, The Astrophysical Journal Supplement Series 235 (2018) 24.

[65] M. Abel, L. Frommhold, X. Li, K. L. Hunt, Infrared absorption by collisional H_2–He complexes at temperatures up to 9000 k and frequencies from 0 to 20 000 cm- 1, The Journal of chemical physics 136 (2012) 044319.

[66] L. O. Anisman, B. Edwards, Q. Changeat, O. Venot, A. F. Al-Refaie, A. Tsiaras, G. Tinetti, Wasp-117 b: An eccentric hot saturn as a future complex chemistry laboratory, The Astronomical Journal 160 (2020) 233. URL: `http://dx.doi.org/10.3847/1538-3881/abb9b0`. doi:`10.3847/1538-3881/abb9b0`.

[67] Q. Changeat, B. Edwards, I. P. Waldmann, G. Tinetti, Toward a more complex description of chemical profiles in exoplanet retrievals: A two-layer parameterization, The Astrophysical Journal 886 (2019) 39. URL: `http://dx.doi.org/10.3847/1538-4357/ab4a14`. doi:`10.3847/1538-4357/ab4a14`.

[68] M. Rocchetto, I. P. Waldmann, O. Venot, P. O. Lagage, G. Tinetti, Exploring Biases of Atmospheric Retrievals in Simulated JWST Transmission Spectra of Hot Jupiters, ApJ 833 (2016) 120. doi:`10.3847/1538-4357/833/1/120`. `arXiv:1610.02848`.

[69] G. Tinetti, P. Drossart, P. Eccleston, P. Hartogh, A. Heske, J. Leconte, G. Micela, M. Ollivier, et al., A chemical survey of exoplanets with ARIEL, Experimental Astronomy 46 (2018) 135–209. doi:`10.1007/s10686-018-9598-x`.

[70] G. Tinetti, P. Eccleston, C. Haswell, P.-O. Lagage, J. Leconte, T. Lüftinger, et al., Ariel: Enabling planetary science across light-years, arXiv e-prints (2021) arXiv:2104.04824. `arXiv:2104.04824`.

[71] B. Edwards, L. Mugnai, G. Tinetti, E. Pascale, S. Sarkar, An Updated Study of Potential Targets for Ariel, The Astronomical Journal 157 (2019) 242. doi:`10.3847/1538-3881/ab1cb9`.

[72] J. P. Gardner, J. C. Mather, M. Clampin, et al., The James Webb Space Telescope, Space Science Reviews 123 (2006) 485–606. doi:`10.1007/s11214-006-8315-7`. `arXiv:astro-ph/0606175`.

[73] N. B. Cowan, T. Greene, D. Angerhausen, et al., Characterizing Transiting Planet Atmospheres through 2025, Publications of the Astronomical Society of the Pacific 127 (2015) 311. doi:`10.1086/680855`. `arXiv:1502.00004`.

[74] L. V. Mugnai, E. Pascale, B. Edwards, A. Papageorgiou, S. Sarkar, ArielRad: the Ariel Radiometric Model, arXiv e-prints (2020) arXiv:2009.07824. `arXiv:2009.07824`.

[75] B. Edwards, I. Stotesbury, Terminus: A Versatile Simulator for Space-based Telescopes, AJ 161 (2021) 266. doi:`10.3847/1538-3881/abdf4d`. `arXiv:2101.10317`.

[76] K. M. Pontoppidan, T. E. Pickering, V. G. Laidler, K. Gilbert, et al., Pandeia: a multi-mission exposure time calculator for JWST and WFIRST, in: A. B. Peck, R. L. Seaman, C. R. Benn (Eds.), Observatory Operations: Strategies, Processes, and Systems VI, volume 9910 of *Society of Photo-Optical Instrumentation Engineers (SPIE) Conference Series*, 2016, p. 991016. doi:`10.1117/12.2231768`. `arXiv:1707.02202`.

[77] G. Tinetti, J. P. Beaulieu, T. Henning, M. Meyer, G. Micela, I. Ribas, D. Stam, M. Swain, O. Krause, M. Ollivier, et al., Echo, Experimental Astronomy 34 (2012) 311–353. URL: `http://dx.doi.org/10.1007/s10686-012-9303-4`. doi:`10.1007/s10686-012-9303-4`.

[78] S. N. Yurchenko, J. Tennyson, J. Bailey, M. D. J. Hollis, G. Tinetti, Spectrum of hot methane in astronomical objects using a comprehensive computed line list, Proceedings of the National Academy of Sciences 111 (2014) 9379–9383. URL: http://dx.doi.org/10.1073/pnas.1324219111. doi:10.1073/pnas.1324219111.

[79] C. Hill, I. E. Gordon, R. V. Kochanov, L. Barrett, L. S. Rothman, HITRANonline: A modern online interface and the flexible representation of spectroscopic data in the HITRAN database, J. Quant. Spectrosc. Radiat. Transf. 177 (2016) 4–14. doi:10.1016/j.jqsrt.2015.12.012.

[80] P. Varanasi, S. Chudamani, The temperature dependence of lineshifts, linewidths and line intensities of methane at low temperatures, J. Quant. Spectrosc. Radiat. Transf. 43 (1990) 1 – 11. doi:10.1016/0022-4073(90)90060-J.

[81] A. S. Pine, Self-, N_2, O_2, H_2, Ar, and He broadening in the ν_3 band Q branch of CH_4, J. Chem. Phys. 97 (1992) 773–785. doi:10.1063/1.463943.

[82] K. Fox, D. E. Jennings, E. A. Stern, R. Hunnard, Measurements of argon-, helium-, hydrogen-, and nitrogen-broadened widths of methane lines near 9000 cm^{-1}, J. Quant. Spectrosc. Radiat. Transf. 39 (1998) 473 – 476. doi:10.1016/0022-4073(88)90092-1.

[83] P. Varanasi, G. D. T. Tejwani, Experimental and theoretical studies on collision-broadened lines in the ν_4-fundamental of methane, J. Quant. Spectrosc. Radiat. Transf. 12 (1972) 849–855. doi:10.1016/0022-4073(72)90073-8.

[84] P. Varanasi, S. Chudamani, Measurements of collision-broadened line widths in the ν_4-fundamental band of $^{12}CH_4$ at low temperatures, J. Quant. Spectrosc. Radiat. Transf. 41 (1989) 335–343. doi:10.1016/0022-4073(89)90062-9.

[85] I. M. Grigoriev, N. N. Filippov, M. V. Tonkov, T. Gabard, R. L. Doucen, Estimation of line parameters under line mixing effects: the ν_3 band of CH_4 in helium, J. Quant. Spectrosc. Radiat. Transf. 69 (2001) 189–204. doi:10.1016/S0022-4073(00)00076-5.

[86] T. Gabard, I. M. Grigoriev, N. M. Grigorovich, M. V. Tonkov, Helium and argon line broadening in the ν_2 band of CH_4, J. Mol. Spectrosc. 225 (2004) 123–131. doi:10.1016/j.jms.2004.02.023.

[87] J. Manne, T. Q. Bui, C. R. Webster, Determination of foreign broadening coefficients for methane lines targeted by the tunable laser spectrometer (TLS) on the mars curiosity rover, J. Quant. Spectrosc. Radiat. Transf. 191 (2017) 59 – 66. doi:10.1016/j.jqsrt.2017.01.035.

[88] E. Gharib-Nezhad, A. N. Heays, H. A. Bechtel, J. R. Lyons, H_2-induced pressure broadening and pressure shift in the P-branch of the $\nu3$ band of CH_4 from 300 to 655 K, J. Quant. Spectrosc. Radiat. Transf. 239 (2019) 106649. doi:10.1016/j.jqsrt.2019.106649.

[89] A. Faure, L. Wiesenfeld, J. Tennyson, B. J. Drouin, Pressure broadening of water and carbon monoxide transitions by molecular hydrogen at high temperatures, J. Quant. Spectrosc. Radiat. Transf. 116 (2013) 79–86. doi:10.1016/j.jqsrt.2012.09.015.

[90] G. Li, I. E. Gordon, L. S. Rothman, Y. Tan, S.-M. Hu, S. Kassi, A. Campargue, E. S. Medvedev, Rovibrational line lists for nine isotopologues of the co molecule in the x $^1\Sigma^+$ ground electronic state, Astrophys. J. Suppl. 216 (2015) 15. doi:10.1088/0067-0049/216/1/15.

[91] C. R. Mulvihill, S. A. Alturaifi, E. L. Petersen, High-temperature He- and O_2-broadening of the R(12) line in the 1-0 band of carbon monoxide, J. Quant. Spectrosc. Radiat. Transf. 217 (2018) 432 – 439. doi:10.1016/j.jqsrt.2018.06.015.

[92] A. Mantz, V. M. Devi, D. C. Benner, M. Smith, A. Predoi-Cross, M. Dulick, A multispectrum analysis of widths and shifts in the 2010–2260 cm- 1 region of 12c16o broadened by helium at temperatures between 80 and 297 k, Journal of Molecular Structure 742 (2005) 99–110.

[93] A. Predoi-Cross, K. Esteki, H. Rozario, H. Naseri, S. Latif, F. Thibault, V. M. Devi, M. Smith, A. Mantz, Theoretical and revisited experimentally retrieved he-broadened line parameters of carbon monoxide in the fundamental band, J. Quant. Spectrosc. Radiat. Transf. 184 (2016) 322–340.

[94] P. Sinclair, P. Duggan, R. Berman, J. R. Drummond, A. May, Line broadening in the fundamental band of co in co–he and co–ar mixtures, J. Mol. Spectrosc. 191 (1998) 258–264.

[95] B. A. Voronin, T. P. Mishina, N. N. Lavrentyeva, T. Y.Chesnokova, V. E. Zuev, M. J. Barber, J. Tennyson, Estimate of the $J'J''$ dependence of water vapor line broadening parameters, J. Quant. Spectrosc. Radiat. Transf. 111 (2010) 2308–2314. doi:`10.1016/j.jqsrt.2010.05.015`.

[96] B. A. Voronin, N. N. Lavrentieva, A. A. Lugovskoy, A. D. Bykov, V. I. Starikov, J. Tennyson, Self- and air-broadening coefficients of HD^{16}O spectral lines, Atmospheric and Oceanic Optics 25 (2012) 27–34. doi:`10.1134/S1024856012010150`.

[97] A. M. Solodov, V. I. Starikov, Broadening and shift of lines of the $\nu_2 + \nu_3$ band of water vapor induced by helium pressure, Optics and Spectroscopy 105 (2008) 14–20. doi:`10.1134/S0030400X08070035`.

[98] A. M. Solodov, V. I. Starikov, Helium-induced halfwidths and line shifts of water vapor transitions of the $\nu_1 + \nu_2$ and $\nu_2 + \nu_3$ bands, Mol. Phys. 107 (2009) 43–51. doi:`10.1080/00268970802698655`.

[99] T. M. Petrova, A. M. Solodov, A. A. Solodov, V. I. Starikov, Vibrational dependence of an intermolecular potential for h$_2$o-he system, J. Quant. Spectrosc. Radiat. Transf. 129 (2013) 241 – 253. doi:`10.1016/j.jqsrt.2013.06.021`.

[100] T. M. Petrova, A. M. Solodov, V. I. Starikov, A. A. Solodov, Measurements and calculations of He-broadening and -shifting parameters of the transitions of the $\nu_1 + \nu_2 + \nu_3$ bands., Mol. Phys. 110 (2012) 1493–1503. doi:`10.1080/00268976.2012.663939`.

[101] T. M. Petrova, A. M. Solodov, A. A. Solodov, V. I. Starikov, Broadening parameters of the H$_2$O-He collisional system for astrophysical applications, J. Mol. Spectrosc. 321 (2016) 50–58. doi:`10.1016/j.jms.2016.01.009`.

[102] R. R. Gamache, B. Vispoel, C. L. Renaud, K. Cleghorn, L. Hartmann, Vibrational dependence, temperature dependence, and prediction of

line shape parameters for the H_2O-H_2 collision system, Icarus 326 (2019) 186 – 196. doi:`10.1016/j.icarus.2019.02.011`.

[103] J. S. Wilzewski, I. E. Gordon, R. V. Kochanov, C. Hill, L. S. Rothman, H_2, He, and CO_2 line-broadening coefficients, pressure shifts and temperature-dependence exponents for the HITRAN database. Part 1: SO_2, NH_3, HF, HCl, OCS and C_2H_2, J. Quant. Spectrosc. Radiat. Transf. 168 (2016) 193 – 206. doi:`10.1016/j.jqsrt.2015.09.003`.

Table 2: Average values of γ and n for various species where parameters are available from HITRAN-2020 [48]. The custom data search from HITRANonline as described in [79] was used in order to extract the relevant parameters. Where ExoMolOP [21] is labelled as the source (where only H_2 and He-broadening was considered), the citations used to find the averaged values are listed in the footnote to this table.

Species	Broadener	γ	n	Source
CO_2	H_2O	0.14	0.79	HITRAN
	Self	0.09	0.64	HITRAN
	Air	0.07	0.71	HITRAN
	H_2	0.11	0.58	HITRAN
	He	0.06	0.3	HITRAN
	H_2	0.09	0.59	ExoMolOP
	He	0.04	0.44	ExoMolOP
CO	H_2O	0.09	0.68	HITRAN
	Self	0.06	-	HITRAN
	Air	0.05	0.7	HITRAN
	CO_2	0.06	0.66	HITRAN
	H_2	0.07	0.58	HITRAN
	He	0.05	0.54	HITRAN
	H_2	0.07	0.65	ExoMolOP
	He	0.05	0.6	ExoMolOP
CH_4	H_2O	0.07	0.85	HITRAN
	Self	0.07	-	HITRAN
	Air	0.05	0.67	HITRAN
	H_2	0.06	0.6	ExoMolOP
	He	0.03	0.3	ExoMolOP
H_2O	Self	0.35	-	HITRAN
	Air	0.07	0.62	HITRAN
	H_2	0.06	0.2	ExoMolOP
	He	0.01	0.13	ExoMolOP

CH_4: [80, 81, 82, 83, 84, 85, 86, 87, 88]
CO: [89, 90, 91, 92, 93, 94]
H_2O: [95, 96, 44, 97, 98, 99, 100, 101, 102]
CO_2 assumed parameters of C_2H_2: [103]